ADVANCED FUNCTIONAL MATERIALS

Supporting Information

for *Adv. Funct. Mater.*, DOI: 10.1002/adfm.201909051

Solid State Fluorination on the Minute Scale: Synthesis of $WO_{3-x}F_x$ with Photocatalytic Activity

*Martin Alexander Lange,1 Yaşar Krysiak,2,3 Jens Hartmann,1 Georg Dewald,4 Giacomo Cerretti,1 Muhammad Nawaz Tahir,5 Martin Panthöfer,1 Bastian Barton,6 Tobias Reich,7 Wolfgang G. Zeier,4 Mihail Mondeshki,1 Ute Kolb,1,2 and Wolfgang Tremel1**

Solid State Fluorination on the Minute Scale: Synthesis of $WO_{3-x}F_x$ with Photocatalytic Activity

Martin Alexander Lange,[1] Yaşar Krysiak,[2,3] Jens Hartmann,[1] Georg Dewald,[4] Giacomo Cerretti,[1] Muhammad Nawaz Tahir,[5] Martin Panthöfer,[1] Bastian Barton,[6] Tobias Reich,[7] Wolfgang G. Zeier,[4] Mihail Mondeshki,[1] Ute Kolb,[1,2] and Wolfgang Tremel[1]*

[1] Institut für Anorganische Chemie und Analytische Chemie, Johannes Gutenberg-Universität Mainz, Duesbergweg 10-14, D-55128 Mainz, Germany

[2] Institut für Angewandte Geowissenschaften, Technische Universität Darmstadt, Schnittspahnstraße 9, 64287 Darmstadt, Germany

[3] Department of Structure Analysis, Institute of Physics, Czech Academy of Sciences, Cukrovarnická 10/112, 162 00 Prague, Czech Republic

[4] Justus-Liebig-University Giessen, Physikalisch-Chemisches Institut, Heinrich-Buff-Ring 17, D-35392 Giessen, Germany

[5] Chemistry Department, King Fahd University of Petroleum and Materials, Dharan 31261, P.O. Box 5048, Kingdom of Saudi Arabia

[6] Fraunhofer LBF, Division Plastics, Schlossgartenstr. 6, D-64289 Darmstadt, Germany

[7] Institut für Kernchemie, Johannes Gutenberg-Universität Mainz, Strassmannweg 2, D-55128 Mainz

Contents

Results of cell parameter analysis via ADT

Table S1. Unit cell parameter values obtained by averaging the lattice parameters of 12 EDT data sets from different crystals of the same sample (SPS prepared $WO_{2.90}F_{0.10}$). Mean values and deviations are calculated neglecting crystal 6 due to complex twinning.

measured crystal	***a* - axis**	**b – axis**	**c – axis**
crystal 1	7.330	7.371	7.714
crystal 2	7.360	7.390	7.712
crystal 3	7.364	7.412	7.725
crystal 4	7.352	7.397	7.717
crystal 5	7.439	7.480	7.678
crystal 6	7.361	7.456	7.717
crystal 7	7.347	7.397	7.726
crystal 8	7.381	7.433	7.720
crystal 9	7.355	7.433	7.711
crystal 10	7.363	7.438	7.693
crystal 11	7.356	7.455	7.735
crystal 12	7.373	7.428	7.751
mean + std. dev.	**7.358 ± 0.013**	**7.419 ± 0.027**	**7.720 ± 0.014**
powder refinement	**7.400**	**7.462**	**7.720**

Table S2. Fit parameter of the three orthorhombic (Figure 4A) and four cubic (Figure 4B) deconvoluted peaks from the F^- solid state MAS NMR of $WO_{2.90}F_{0.08}$ (conventional synthesis)/$WO_{2.90}F_{0.10}$ (SPS-prepared) and $WO_{2.60}F_{0.40}$ (conventional synthesis)/ $WO_{2.40}F_{0.60}$ (SPS-prepared).

SPS – orthorh. (Figure S6A)	**Peak 1**	**Peak 2**	**Peak 3**	**Peak 4**
Peak position / ppm	-136.0	-113.7	-109.0	
FWHM / ppm	26.0	3.9	12.2	
Relative peak area	65 %	24 %	11 %	
Conv. – orthorh. (Figure S6A)				
Peak position / ppm	-138.0	-112.4	-105.2	
FWHM / ppm	28.0	4.8	12.0	
Relative peak area	50 %	35 %	15 %	
SPS – cubic (Figure S6B)				
Peak position / ppm	-138.0	-108.5	-99.3	-94.7
FWHM / ppm	28.0	6.6	5.8	15.6
Relative peak area	39 %	43 %	5 %	13 %
Conv. – cubic (Figure S6B)				
Peak position / ppm	-146.0	-108.2	-102.4	94.6
FWHM / ppm	22.0	7.1	2.2	3.8
Relative peak area	32 %	48 %	8 %	13 %

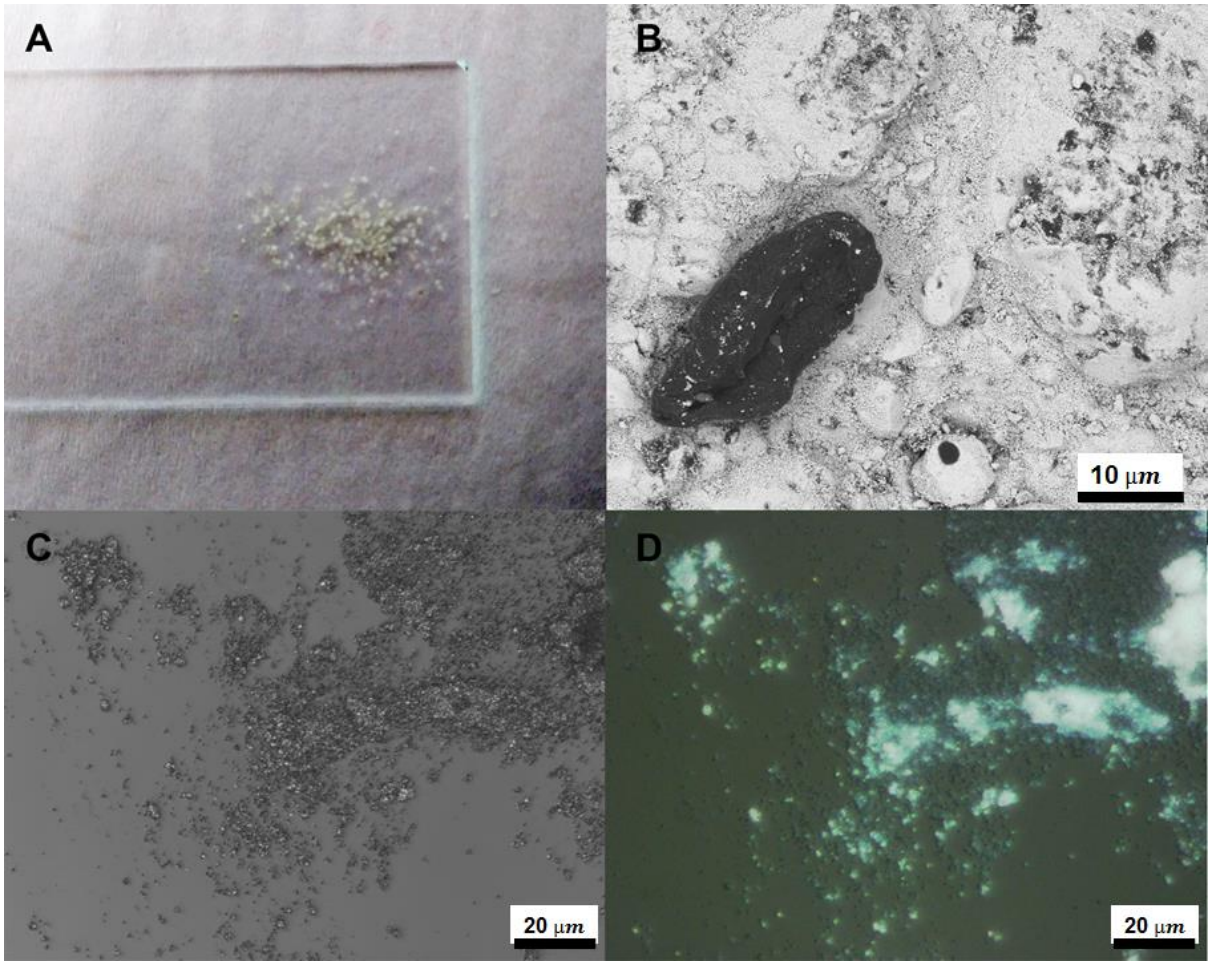

Figure S1. Flake-like structures formed after ball-milling powder mixtures with high PTFE/WO_3 ratios **(A+C+D)** and pellet cross-section of not ball-milled precursor mixture (**B**). The black particles in the SEM image consist of PTFE-remnants that were formed when mixing of the PTFE and WO_3 precursors was insufficient (e.g. no ball-milling) and result from incomplete PTEF decomposition and reaction with WO_3. These particles are responsible for "pores" in product pellets after the reaction.

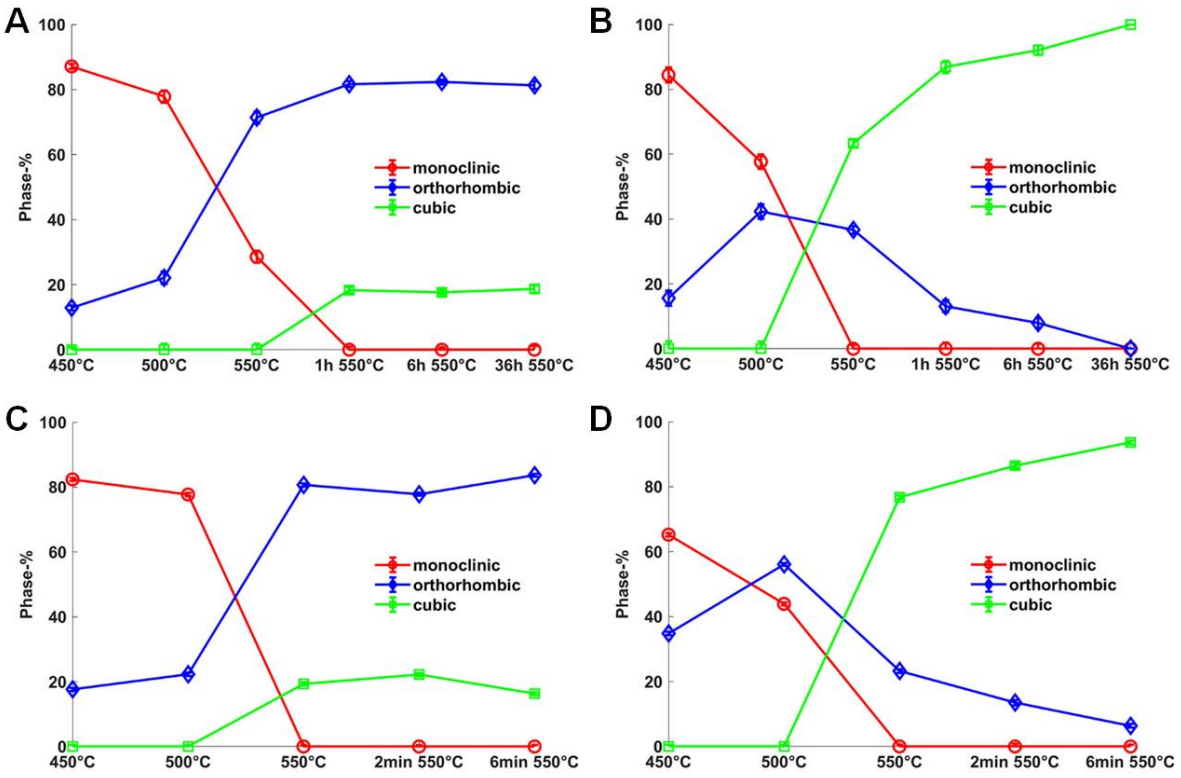

Figure S2. Evolution of $WO_{3-x}F_x$ monoclinic, orthorhombic and cubic phases during the SPS reaction for two different starting compositions x = 0.15 (**A + C**) and x = 1.0 (**B + D**). Analyses were carried out by stopping the reaction at the indicated points of the reaction on the x axis. The progress of the SPS reaction is shown in **C+D** and that of the conventional synthesis in **A+B**.

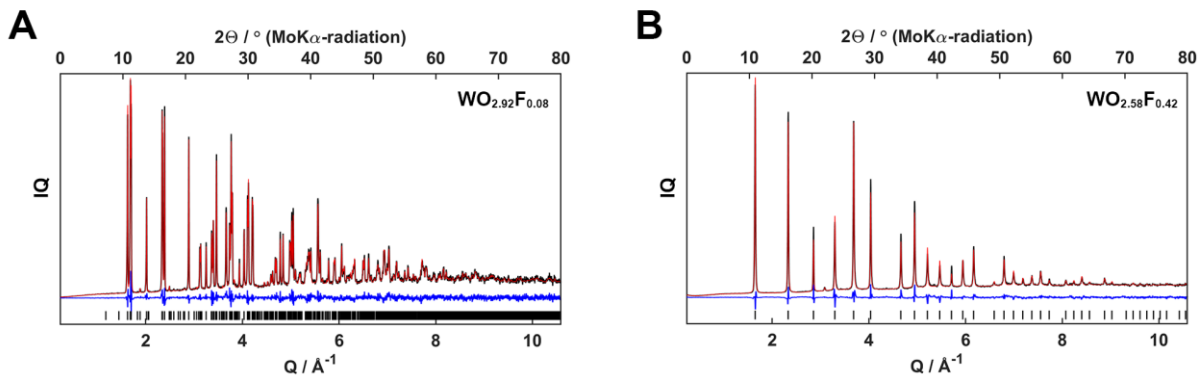

Figure S3. Rietveld Refinements of phase pure conventional sample $WO_{2.92}F_{0.08}$ (**A**) and $WO_{2.60}F_{0.40}$ (**B**). Intensities are weighted with Q-values.

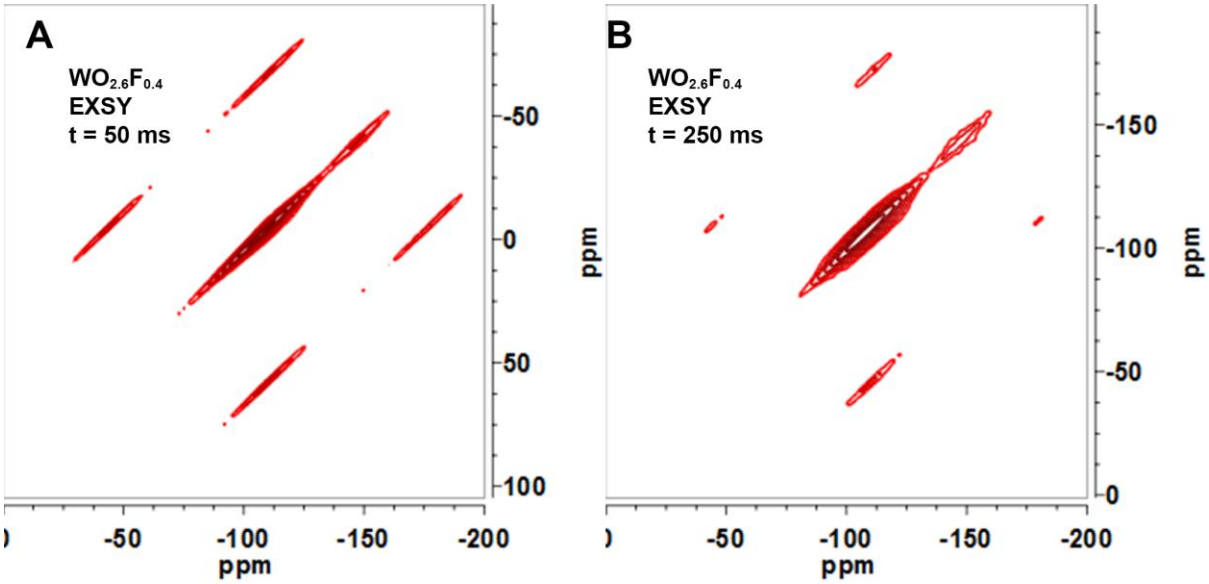

Figure S4. (**A**) ^{19}F EXSY solid state spectrum of cubic $WO_{2.6}F_{0.4}$ at t_{mix} = 50 ms. Three to four distinct fluorine environments were identified. Two to three between 100 and 120 ppm and one at 148 ppm. (**B**) ^{19}F EXSY solid state spectrum of cubic $WO_{2.6}F_{0.4}$ at t_{mix} = 250 ms. Three to four distinct fluorine environments were identified. All fluorine environments are independent due to the absence of cross correlation. Spinning side bands at 45 ppm and 180 ppm are correlated to the fluorine signal at approx. 110 ppm.

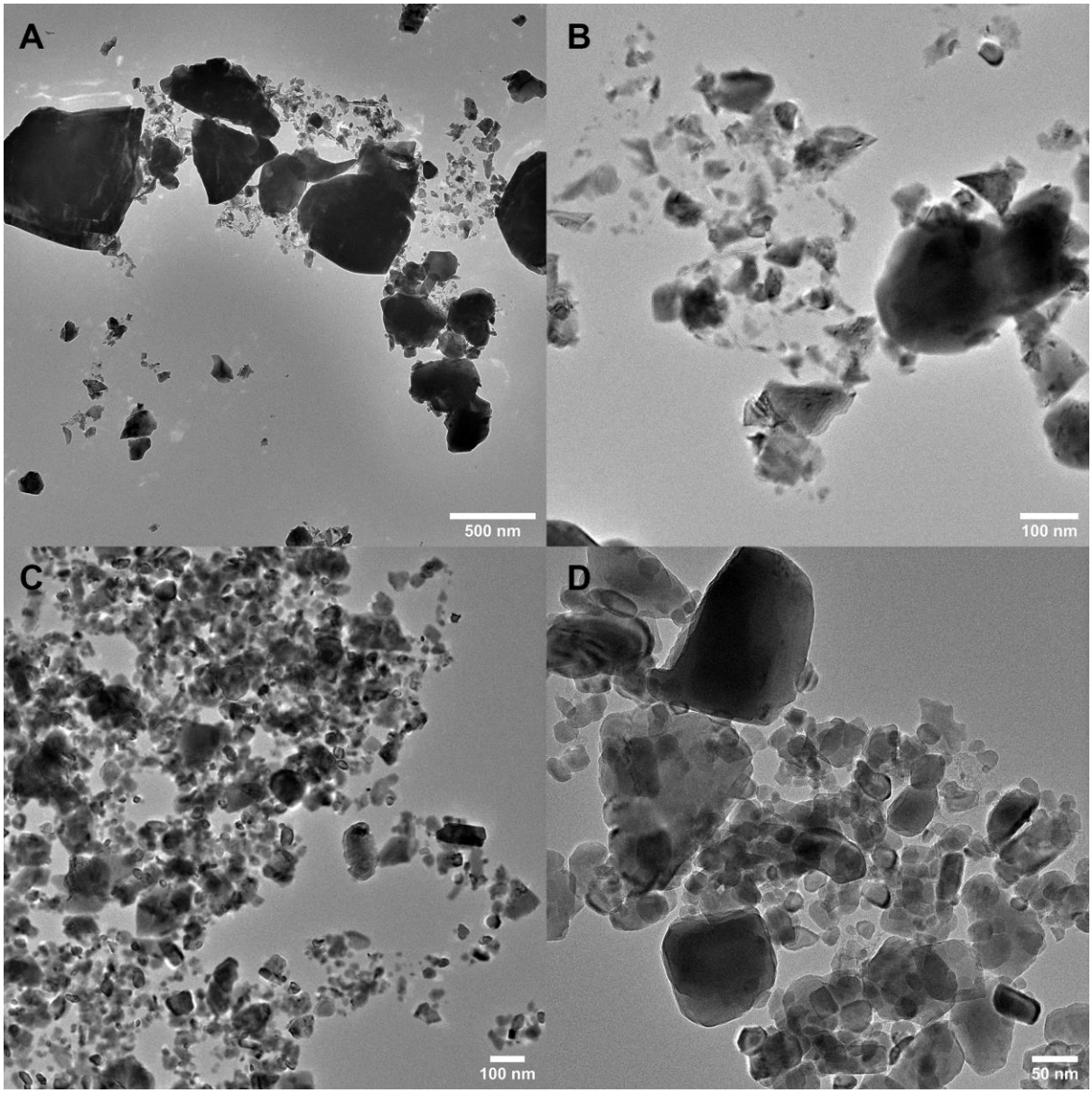

Figure S5. Overview TEM image for conventionally synthesized $WO_{2.58}F_{0.42}$ (**A** + **B**) and SPS-prepared $WO_{2.40}F_{0.60}$ (**C** + **D**) using identical procedure for mixing by ball-milling prior to the reactions. The grains in the SPS-prepared sample are more uniform and smaller than in the conventionally-prepared sample.

X-ray photoelectron spectroscopy (XPS). For additional XPS measurements of air heated samples, powders were pressed into indium foil and transferred into the XPS spectrometer (SPECS GmbH, Germany). When the pressure inside the vacuum chamber was below 5×10^{-8} mbar, the spectra were recorded using both non-monochromatized Al Kα radiation (1486.6 eV) and Mg Kα radiation (1253.6 eV) from the twin-anode X-ray source XR 50, which was operated at 10 kV and 10 mA. To measure a survey spectrum, the hemispherical energy analyzer PHOIBOS 100 was operated at constant analyzer pass energy Ep = 50 eV. High-resolution spectra of W 4f and 5p, and O 1s were recorded with ten sweeps, F 1s with 50 sweeps each at Ep = 13 eV.

CasaXPS (Casa Software Ltd., UK) was used for XPS data analysis. After subtraction of the X-ray satellites and calculation of the background according to Shirley, the individual spectral components of the W 4f and 5p, F 1s, and O 1s spectra were fitted using a product of a Gaussian function with a Lorentzian (GL(60)).

Results of XPS spectroscopy of air heated $WO_{3-x}F_x$ samples

Figure **S5** and **S6** show the F (**A+D**), O (**B+E**), and W (**C+F**) regions of the XPS spectra of $WO_{2.9}O_{0.1}$ (**S5**) and $WO_{2.55}O_{0.45}$ (S6) synthesized by SPS (**A-C**) and conventionally (**D-F**). The XPS overview spectrum (**Figure S4**) confirms the presence of the elements W, O, and F. Furthermore the absence of Carbon after air heating can be confirmed. In **Figure S5/6 C and F**, the peaks centered at 36 and 39 eV are assigned to the W 4f 7/2 and W 4f 5/2 orbitals, respectively, revealing the oxidation states of VI for $WO_{2.9}F_{0.1}$ and $WO_{2.55}O_{0.45.}$ Independent of the synthesis method. No W(V) states could be clearly identified leading to the conclusion that the particle surface gets at least partially oxidized during air-heating. Fitting the W 4f orbitals leaves a small residue which could indicate a small amount W(V) states. The O 1s areas in **Figure S5/6 B and E** show two signals at 531 and 533 eV for conventional synthesized samples, which correspond to lattice O and surface hydroxyl groups. Compared to **Figure 6**, surface water was completely removed and for SPS synthesized samples, surface hydroxyl was be removed too. The XPS spectra of the F 1s core electrons (**Figure 6A and D**) show a signal centered at 685 eV, originating from W− F bonds on the surface of the tungsten oxyfluoride samples. A second F 1s peak at 687 eV, only present in the spectrum of the oxyfluoride synthesized conventionally, is assigned to substitutional F atoms that occupy oxygen sites in the lattice with their associated W− O− H bonds.

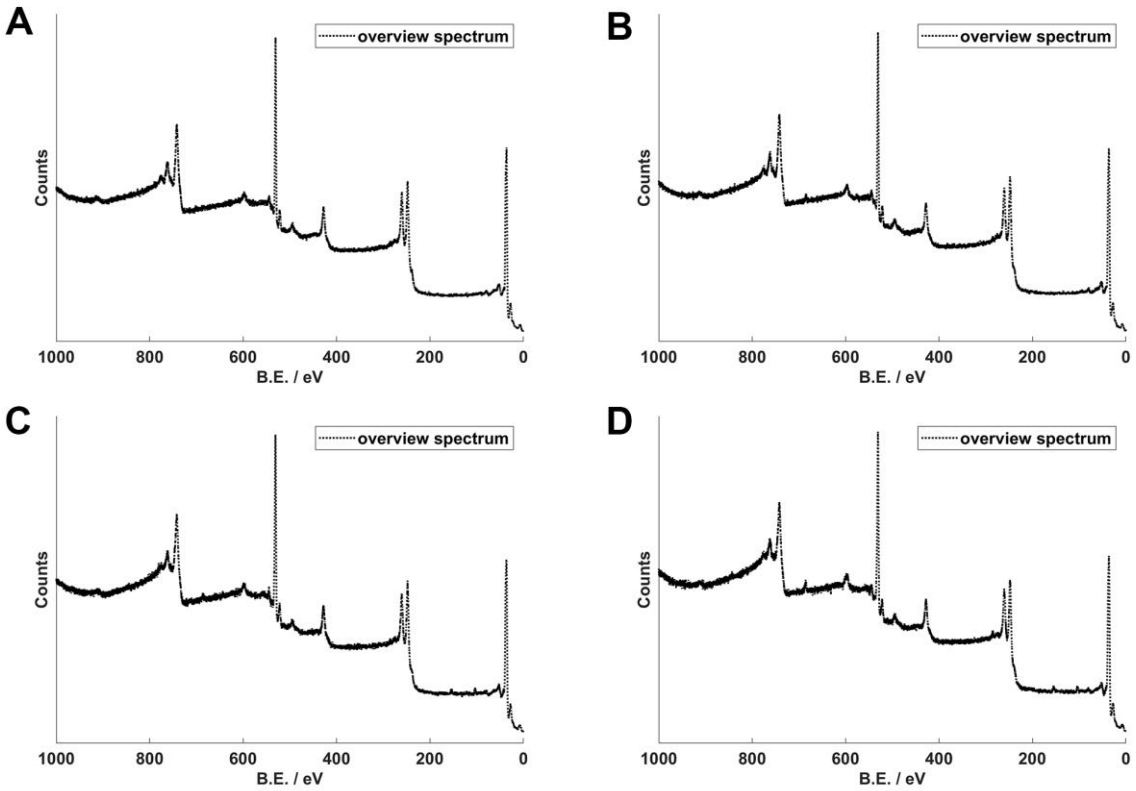

Figure S6. XPS overview spectra of conventional (**C,D**) and SPS (**A,B**) synthesized orthorhombic $WO_{2.90}O_{0.10}$ (**A,C**) and cubic $WO_{2.60}O_{0.40}$ (**B,C**).

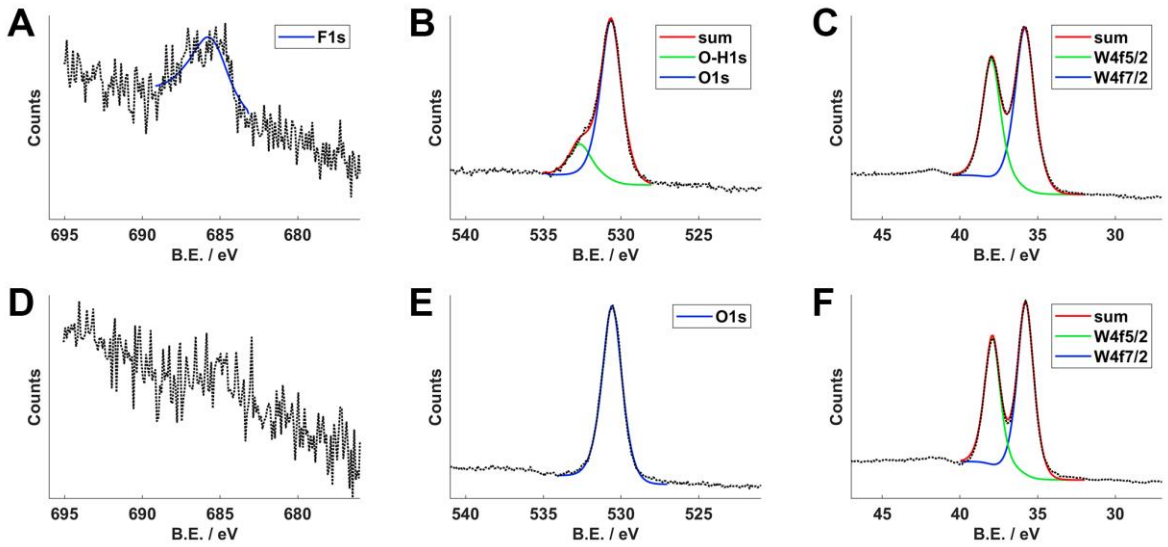

Figure S7. Fitted XPS spectra of conventionally (**A-C**) and SPS (**D-F**) prepared orthorhombic $WO_{2.90}O_{0.10}$. The F, O, and W sub-spectra are shown in (**A,D**), (**B,E**) and (**C,F**).

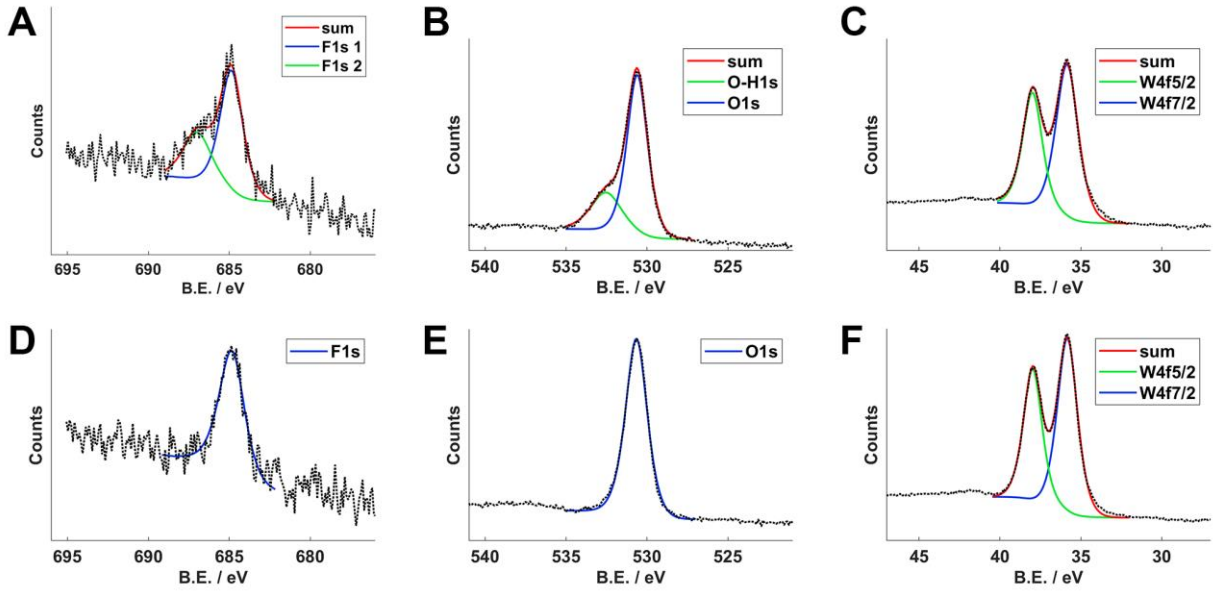

Figure S8. Fitted XPS spectra of conventionally (**A-C**) and SPS (**D-F**) prepared cubic $WO_{2.60}O_{0.40}$. The F, O, and W sub-spectra are shown in (**A,D**), (**B,E**) and (**C,F**).

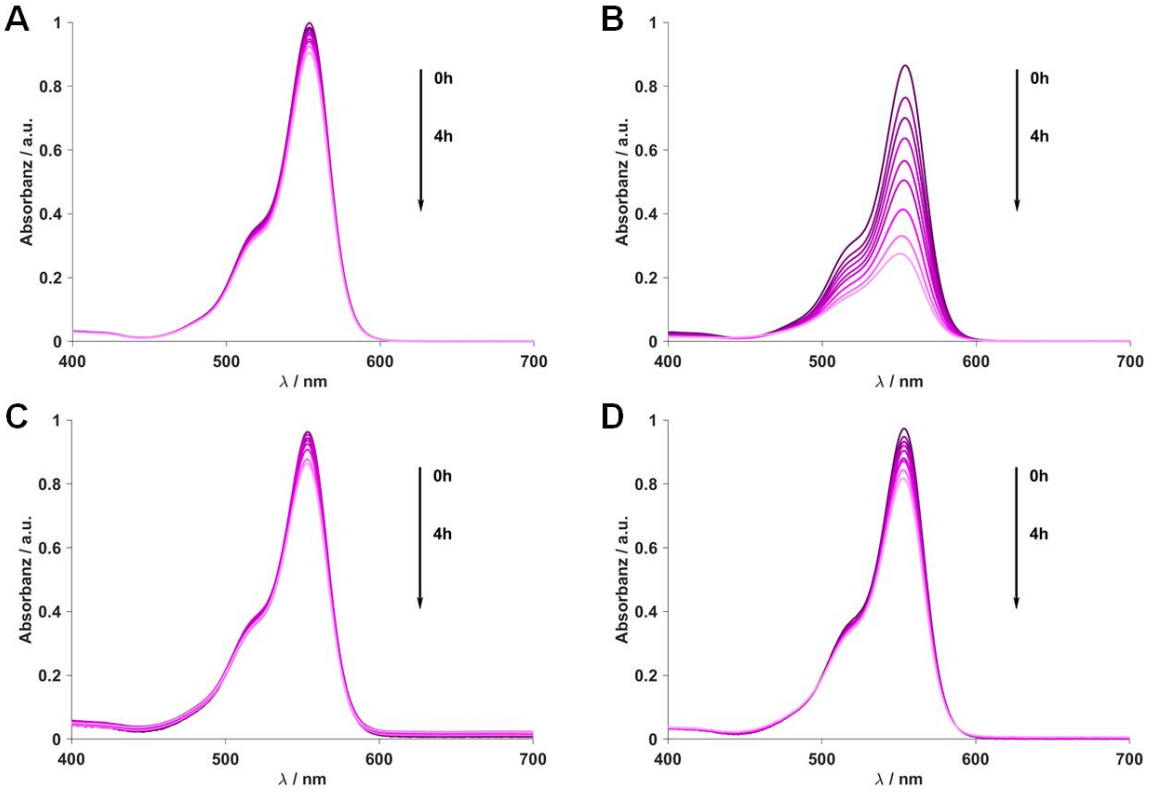

Figure S9. UV−vis spectra showing the photocatalytic degradation of RhB in aqueous solution for cubic (**A + B**) and orthorhombic (**C + D**) $WO_{3-x}F_x$ prepared by conventional solid state chemistry (**A** - $WO_{2.60}F_{0.40}$**, C** - $WO_{2.92}F_{0.82}$) and by SPS (**B** - $WO_{2.40}F_{0.60}$**, D**- $WO_{2.90}F_{0.10}$).

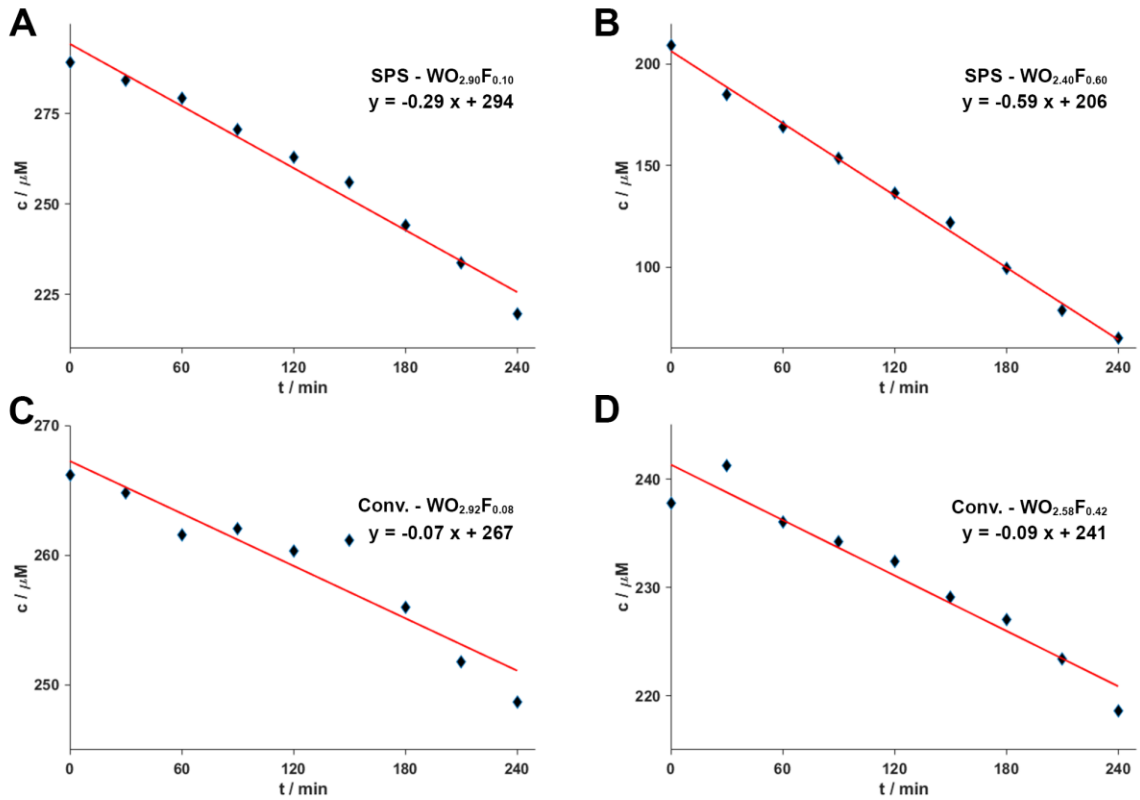

Figure S10. Plots showing the concentration development of RhB during photocatalytic degradation in aqueous solution for $WO_{2.55}O_{0.45}$ (**B + D**) and $WO_{2.9}F_{0.1}$ (**A + C**) prepared by conventional solid state chemistry (**C, D**) and by SPS (**A, B**).

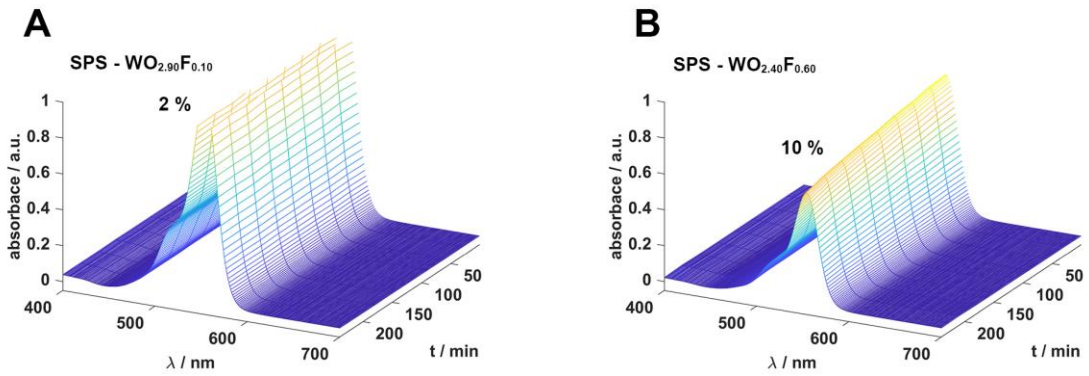

Figure S11. UV−vis spectra showing the photocatalytic degradation of RhB in aqueous solution under dark conditions for SPS prepared orthorhombic $WO_{2.90}F_{0.10}$ (**A**) and cubic $WO_{2.40}F_{0.60}$ (**B**).